



Subscriber access provided by University of Puerto Rico - Mayaguez - Library

Article

Highly efficient deoxydehydration and hydrodeoxygenation on MoS2supported transition metal atoms through a C-H activation mechanism

Yongjie Xi, and Andreas Heyden

ACS Catal., Just Accepted Manuscript • DOI: 10.1021/acscatal.0c02669 • Publication Date (Web): 31 Jul 2020

Downloaded from pubs.acs.org on August 4, 2020

Just Accepted

"Just Accepted" manuscripts have been peer-reviewed and accepted for publication. They are posted online prior to technical editing, formatting for publication and author proofing. The American Chemical Society provides "Just Accepted" as a service to the research community to expedite the dissemination of scientific material as soon as possible after acceptance. "Just Accepted" manuscripts appear in full in PDF format accompanied by an HTML abstract. "Just Accepted" manuscripts have been fully peer reviewed, but should not be considered the official version of record. They are citable by the Digital Object Identifier (DOI®). "Just Accepted" is an optional service offered to authors. Therefore, the "Just Accepted" Web site may not include all articles that will be published in the journal. After a manuscript is technically edited and formatted, it will be removed from the "Just Accepted" Web site and published as an ASAP article. Note that technical editing may introduce minor changes to the manuscript text and/or graphics which could affect content, and all legal disclaimers and ethical guidelines that apply to the journal pertain. ACS cannot be held responsible for errors or consequences arising from the use of information contained in these "Just Accepted" manuscripts.

Highly efficient deoxydehydration and hydrodeoxygenation on MoS₂-supported transition metal atoms through a C-H activation mechanism

Yongjie Xi and Andreas Heyden*

Department of Chemical Engineering, University of South Carolina, 301 South Main Street, Columbia,

South Carolina 29208, United States

Abstract: Deoxydehydration (DODH) is an efficient process for the removal of vicinal OH groups of a diol or polyol. Conventional DODH reactions usually take place at a single-site MO_x (M=Re, Mo, V etc.) active center, which proceed through a diol condensation step, an alkene extrusion step and a catalyst regeneration (or reduction) step. Here, we suggest that MoS₂-supported transition metal atoms allow for the DODH reaction to occur through an alternative mechanism, whereby the C-H bond of a diol is activated first, which facilitates the C-OH bond cleavage on a neighboring carbon. The removal of the second OH group is also facile over the proposed catalysts. Our kinetic studies suggest that the DODH of ethylene glycol on Ru₂/MoS₂, Ir₂/MoS₂ and Ru₃/MoS₂ are highly active with predicted turnover frequencies of over 1/s. Thus, our study suggests a possible approach for the design of highly active DODH catalysts. Apart from being a DODH catalyst, the proposed MoS₂-supported catalysts are also highly active as hydrodeoxygenation catalyst for the removal of alcohol OH groups.

Keywords: deoxydehydration, MoS₂, C-H activation, C-OH cleavage, hydrodeoxygenation, DFT calculations.

1. Introduction

Searching for alternative energy sources to fossil fuels is essential to achieve sustainability. The conversion of biomass into fuels and chemicals have received considerable interest during the past decade. However, biomass-derived raw materials are usually oxygen-rich, making it necessary to develop efficient deoxygenation catalysts. Among various deoxygenation processes, there is a surge of interest in deoxydehydration, which removes vicinal OH groups of a diol and converts it into an alkene. Cook and Andrews' seminal work in 1996 reported a homogeneous Re-catalyzed DODH reaction. To reduce the cost of rhenium compounds, Mo-16 and V-based Thomogeneous catalysts have been developed. The DODH catalyst was heterogenized by supporting ReO_x on activated carbon in 2013. Ensuing studies suggested that CeO₂11 and TiO₂12 can better stabilize the ReO_x species than activated carbon. Experimental and computational studies in heterogeneous DODH catalysts have been abundant in recent years. Among them, most of the reported heterogeneous DODH catalysts feature a supported single-site MO_x (M=Re, Mo, V etc.) catalytic center. Recently, unsupported rhenium oxide nanoparticles have been reported as DODH catalyst with 3-octanol as the reductant.

Typically, the mechanism of a DODH process involves three steps. First, the two O-H bonds of a diol are cleaved sequentially, forming a diolate species adsorbed on a catalyst. Accompanied with the breaking of the O-H bonds, a water molecule is formed by the hydrogen atoms from the diol and the oxygen atom of the MO_x (M=Re, Mo, V et.al) species. Second, the two C-O bonds of the diolate are broken, forming an alkene. The alkene extrusion step leaves an additional oxygen on the catalyst. Third, the catalyst is regenerated by a reductant. While PPh₃ and alcohols are commonly used reductants, H₂ is arguably a more economically viable alternative to them. Utilization of H₂ as the reductant in DODH requires a co-catalyst which plays the role of H₂ activation. For example, Pd serves as a co-catalyst in a ReO_x-Pd/CeO₂ catalyst. Since Pd is a hydrogenation catalyst, the formed alkene is hydrogenated readily over ReO_x-Pd/CeO₂. Whereas the reduction step may occur prior to the extrusion, it is well-accepted that all three steps are necessary to complete the DODH catalytic cycle.

To design a novel heterogeneous DODH catalyst, we explore if it is possible to remove vicinal OH groups through a new mechanism different from the above-mentioned three-step mechanism. The concept of single-atom catalysis has aroused enormous interest in heterogeneous due to the high atom efficiency, reaction activity and selectivity to desired products.²¹⁻²⁴ Atom-pair catalysts, for which two neighboring single atoms work synergistically, allow for the reaction to occur in a different mechanism

from the single-atom counterpart and opens more possibilities for the design of novel catalysts. 25-30

In the present study, we apply the concept of atom-pair catalysts to the design of a DODH catalyst. We examine the DODH reaction pathways on two-dimensional MoS₂-supported transition metals. MoS₂ was employed since sulfur vacancies, serving as anchoring site of transition metals, can be readily created on the basal planes of MoS₂ through hydrogen annealing, electrochemical desulfurization or H₂O₂ chemical etching.³¹⁻³³ The S-vacancy of MoS₂ can be used to stabilize a single-atom catalyst, which was explored in experimental and computational studies. 31, 34-35 The two-dimensional form of MoS₂ is used since it exposes more basal plane sites than its bulk counterpart. In the alkene extrusion process of the conventional DODH mechanism, the two C-O bonds break in one elementary step after O-H bond dissociation. 13-14 Here, we explore the possibility of cleaving the C-OH bonds step-by-step (C1-O1 and C2-O2 in Figure 1a) on MoS₂-supported atom-pair catalysts which leads to the DODH of a diol. Since transition metals may activate the C-H bond of a diol, we also incorporate the C-H activation (C1-H3 and C2-H4 in Figure 1a) process in our mechanistic study. The C-H activation is followed by C-OH bond cleavage at a neighboring carbon atom. To our knowledge, no previous study explored the DODH reaction through a C-H activation mechanism. Specifically, we show that while the activity of the ethylene glycol (EG) C-O (or C-OH) bond cleavage on Ru₁/MoS₂ or Ir₁/MoS₂ is relatively low, Ru₂/MoS₂ or Ir₂/MoS₂ allows for the DODH reaction to occur with high activity through a C-H activation mechanism. Since multiple sulfur vacancies can be created on MoS₂, 31 we also examined the catalytic DODH reaction on Ru₃/MoS₂ and Ir₃/MoS₂, where three S-vacancies are created to accommodate Ru₃ or Ir₃, which are shown to be active for the removal of EG hydroxyl groups. It should be mentioned that the MoS₂-suppored Ru₂, Ru₃, Ir₂ and Ir₃ are significantly more stable than the corresponding supported single-atoms (see Figure S1). Next, a microkinetic model was developed to gain further insights into the reaction mechanism and rate controlling steps. To compare the activity of C-OH bond cleavage occurring after C-H activation and direct C-OH bond cleavage, we also examined the two processes on Pt₂/MoS₂ and Rh₂/MoS₂.

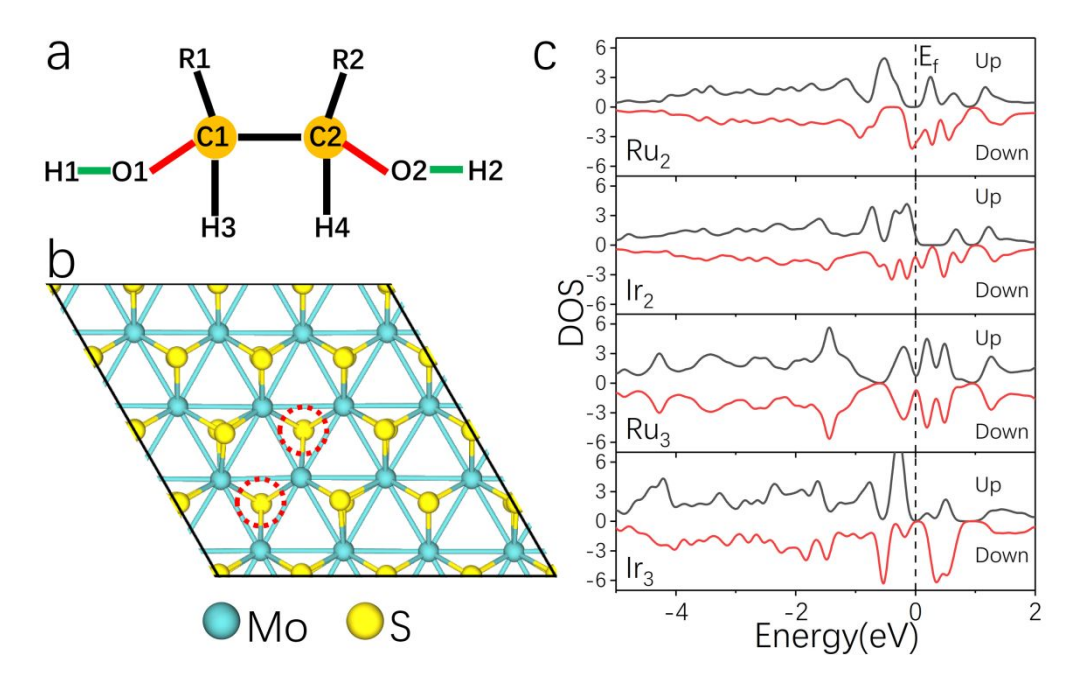


Figure 1. a. Labelling of atoms of a diol. **b.** Configuration of a (4×4) MoS₂ supercell with two S vacancies. **c.** Project density of states for Ru and Ir in Ru₂/MoS₂, Ir₂/MoS₂, Ru₃/MoS₂ and Ir₃/MoS₂. The position of S vacancy is marked by red dashed circle.

2. Computational methods

First-principles calculations were performed using periodic density functional theory (DFT), as implemented in the Vienna Ab initio Simulation Package (VASP 5.4.4). $^{36-37}$ The spin-polarized generalized gradient approximation (GGA) with the PBE functional 38 was used to treat exchange—correlation effects. A plane wave basis set with a cutoff energy of 400 eV was selected to describe the valence electrons. The electron—ion interactions were described by the projector augmented wave (PAW) $^{39-40}$ method. Brillouin zone integration was performed with a $3\times3\times1$ Monkhorst—Pack 41 (MP) k-mesh and Gaussian smearing (σ =0.1 eV). We used Grimme's DFT-D3 42 scheme to treat the van der Waals interactions semi-empirically. The SCF and force convergence criteria for structural optimization were set to 1×10^{-5} eV and 0.01 eV/Å, respectively. The climbing image nudged elastic band (CI-NEB) 43 and dimer methods $^{44-45}$ were used to optimize the transition state structures to achieve a force criteria of 0.03 eV/Å. All transition states have been confirmed with existence of one imaginary frequency whose corresponding eigenvector points in the direction of the reactant and product state. Neighboring slabs were separated by at least 15 Å vacuum. The adsorption energy of a gas phase molecule is defined as $E_{ads} = E(surface+adsorbent) - E(surface) - E(adsorbent)$. The two-dimensional

 MoS_2 is represented by a (4×4) slab (see Figure 1b), where two S-vacancies are created to accommodate Ru_2 and Ir_2 . The calculated lattice parameter of MoS_2 is 3.17 Å which is close to the experimental value of 3.16 Å.⁴⁶

Harmonic transition state theory was used to calculate all elementary rate constants of surface processes. Collision theory with a sticking coefficient of 1 was used to estimate the rate constants for adsorption processes. Details of the calculated rate constants and the microkinetic models are provided in the supporting information.

3. Results and discussions

3.1 C-O bond cleavage through different mechanisms on Ru₁/MoS₂ and Ir₁/MoS₂

We first calculated the (dissociative) chemisorption free energies (Table S1) of EG and H₂ on MoS₂-supported Ru₁-Ru₃ and Ir₁-Ir₃ at 423K to examine the preference of EG and H₂ adsorption on each surface. Ir₂/MoS₂ can accommodate two H₂ molecules while all other MoS₂-supported Ru/Ir atom(s) can accommodate only one H₂ molecule. The EG molecule can be chemisorbed on a supported metal site or physiosorbed on a basal plane site (Figure S2) while the metal site is preferred over the basal plane site in all cases and the calculated adsorption energy difference is ca. 0.6 eV. The adsorption free energy of EG is more negative than that of H₂ in each case, suggesting that catalyst poisoning by hydrogen is minimal. Next, Figure 2 illustrates that the C-O bond cleavage of EG on Ru₁/MoS₂ and Ir₁/MoS₂ through direct C-OH cleavage (C1-O1 in Figure 1a) has high barriers of over 1.5 eV, which are difficult to overcome at typical DODH reaction conditions of around 423 K. 13, 15 In the O-H scission mechanism, the two O-H bonds (O1-H1 and O2-H2 in Figure 1a) of EG are cleaved at the Ru₁ or Ir₁ site, followed by ethylene extrusion (C1-O1 and C2-O2 are broken concurrently). All of these elementary steps are endergonic and possess high barriers on both Ru₁/MoS₂ and Ir₁/MoS₂. Initial C-H activation prior to C-OH bond cleavage (C1-H3 bond cleavage, followed by C2-O2 bond cleavage in Figure 1a) reduces the effective barrier relative to direct C-OH cleavage, however, the effective barrier remains relatively high, i.e., it is 1.46 eV for Ru₁/MoS₂ and 1.14 eV for Ir₁/MoS₂. Therefore, Ru₁/MoS₂ and Ir₁/MoS₂ are not good candidates as highly active DODH catalysts for EG. We next investigate the catalytic DODH of EG on MoS₂-supported Ru and Ir atom-pairs.

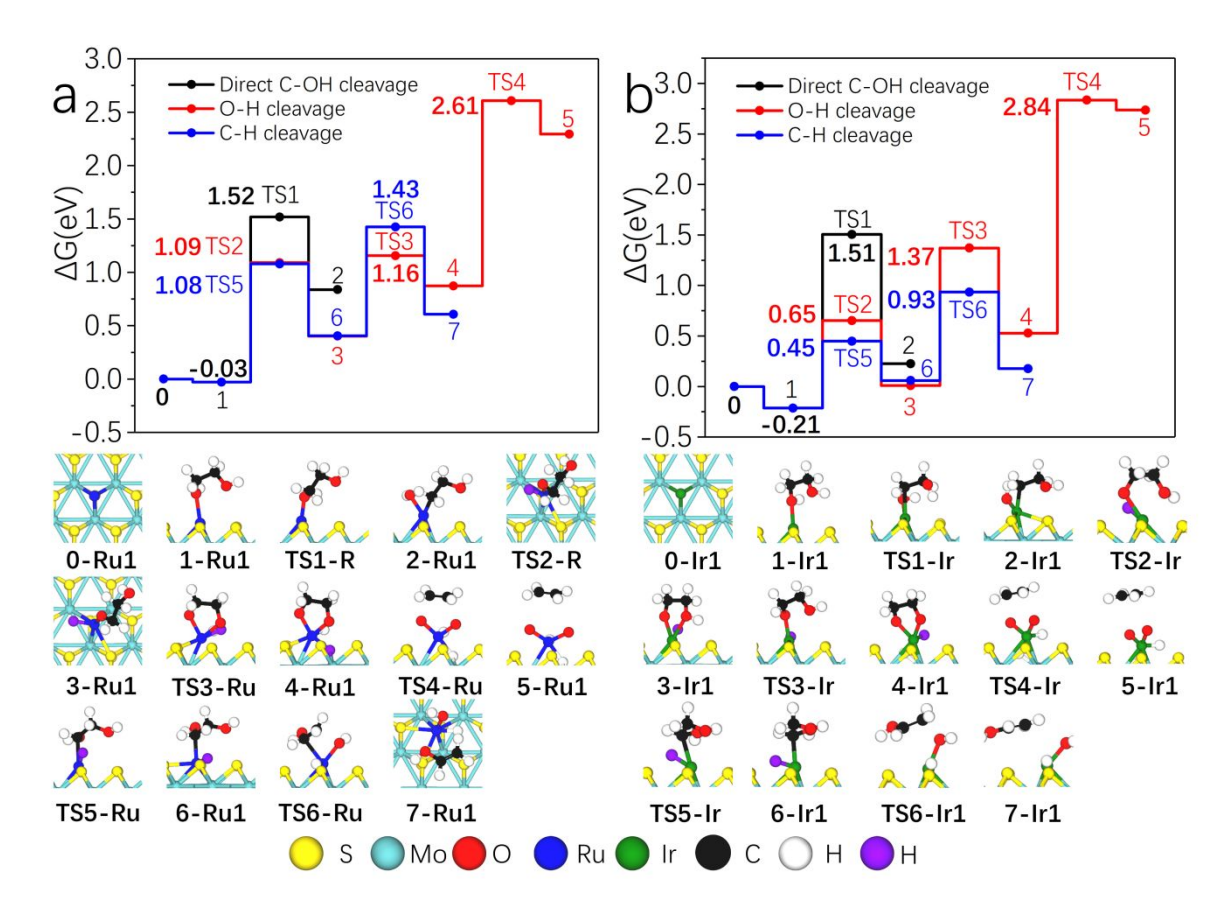


Figure 2. Free energy profiles of the EG C-O bond cleavage through the direct C-OH cleavage, O-H cleavage and C-H cleavage mechanism on Ru₁/MoS₂(a) and Ir₁/MoS₂(b) at 423 K. The partial pressures of all gas phase molecules are set to be 1 bar. Each elementary step is also described in Table S2.

3.2 DODH of EG on Ru₂/MoS₂

To examine the reactivity of the DODH of EG on Ru_2/MoS_2 , we considered the reactions proceeding through direct C-OH cleavage, O-H scission followed by ethylene extrusion, as well as the C-H activation pathways. The projected density of states to the Ru atoms suggest that there is a population of states near the Fermi level (Figure 1c), which is favorable for electron transfer from Ru_2 to the EG molecule, leading to a relatively strong adsorption (E_{ads} , no zero-point energy correction is applied) of EG of -1.04 eV. This is also true for the cases of Ir_2 , Ru_3 and Ir_3 (Ir_2 , -1.42 eV; Ru_3 , -1.19 eV; Ir_3 , -1.31 eV). The free energy profiles of each process were calculated at 423 K and are shown in Figure 3 and 4. The direct C-OH cleavage ($1-Ru_2 \rightarrow 2-Ru_2$) can occur on Ru_2/MoS_2 with a moderately high effective barrier of 1.01 eV. The dissociative adsorption of an H_2 molecule on $2-Ru_2$ forms $3-Ru_2$, which produces a H_2O molecule ($4-Ru_2$) upon the association of H and OH by overcoming a vanishingly small free energy barrier. Upon desorption of H_2O , the leftover H atom can form ethanol ($5-Ru_2 \rightarrow 6-Ru_2 \rightarrow 6-Ru_2$

 $\mathbf{R}\mathbf{u}_2$) or migrate to the other Ru site (5- $\mathbf{R}\mathbf{u}_2 \rightarrow 7$ - $\mathbf{R}\mathbf{u}_2$) readily. The dissociation of the ethanol O-H bond is energetically uphill by 0.23 eV ($6-Ru_2\rightarrow 24-Ru_2$), as displayed in Figure S3. The cleavage of another C-OH bond is concomitant with the formation of $H_2O(7-\mathbf{Ru}_2 \rightarrow 8-\mathbf{Ru}_2)$, which only requires overcoming a low barrier of 0.04 eV. Meanwhile, the effective barrier of (6-Ru₂→5-Ru₂→7-Ru₂) is calculated to be 0.72 eV, suggesting that the formed ethanol molecule can be further deoxygenated readily. 8-Ru₂ \rightarrow $9-Ru_2$ corresponds to the desorption of the second H_2O . The ethylene molecule can desorb endergonically $(9-Ru_2\rightarrow 0-Ru_2)$ or undergo a hydrogenation process $(9-Ru_2\rightarrow 14-Ru_2)$ which includes the first hydrogen migration step (10-Ru₂ \rightarrow 11-Ru₂), the first hydrogenation step (11-Ru₂ \rightarrow 12-Ru₂), the second hydrogen migration step (12-Ru₂ \rightarrow 13-Ru₂) and the second hydrogenation step (13-Ru₂ \rightarrow 14-Ru₂). The effective barrier of ethylene hydrogenation is calculated to be 0.85 eV. Upon desorption of ethane, the catalytic cycle through the direct C-OH cleavage pathway is closed. Since the activation energy of the C-OH bond cleavage can be affected by the presence of H₂O,⁴⁷ we also investigated the effect of H₂O on the kinetics of the C-OH bond cleavage. As shown in Figure S4, the direct C-OH bond cleavage has a higher effective barrier in the presence H₂O than the absence of it. Since the adsorption of H₂O is endergonic and the H₂O-participated pathway is energetically uphill, the kinetics of the direct C-OH is essentially unaffected by H₂O.

The cleavage of the first EG O-H bond ($1\text{-Ru}_2 \rightarrow 15\text{-Ru}_2$) on Ru_2/MoS_2 requires overcoming a relatively low barrier of 0.69 eV and is exergonic by 0.25 eV (Figure 3b). The cleavage of the second O-H requires surmounting a barrier of 1.60 eV and the extrusion of ethylene is highly endergonic. The effective barrier of the reaction along the O-H bond breaking pathway is 2.30 eV, suggesting that the conventional DODH mechanism is unfavorable for the EG DODH on Ru_2/MoS_2 .

We next examined the DODH of EG through a C-H activation mechanism. Our calculations suggest that the C-H activation of EG can occur readily on Ru_2/MoS_2 by only overcoming a barrier of 0.59 eV on one Ru atom ($1-Ru_2\rightarrow 18-Ru_2$ in Figure 3c). The abstracted hydrogen atom can migrate to the other Ru atom ($18-Ru_2\rightarrow 19-Ru_2$) and form readily a H₂O molecule with the OH group of EG ($19-Ru_2\rightarrow 20-Ru_2$). The dissociative chemisorption of H₂ occurs on $21-Ru_2$, which forms $22-Ru_2$. Next, one H atom is added to the α -C of ethenol ($22-Ru_2\rightarrow 23-Ru_2$), whose forward free energy barrier is the endothermicity of the reaction (i.e., the backward energy barrier is vanishingly small). The formed CH₂CH₂OH radical ($23-Ru_2$) can migrate towards the Ru atom with the adsorbed hydrogen, which produces $5-Ru_2$. The remaining part of the DODH reaction through the C-H activation mechanism is

the same as that through the C-OH scission mechanism. Considering the energy profiles of the three DODH mechanisms, we conclude that the C-H activation prior to C-OH cleavage can greatly facilitate the ensuing C-OH bond cleavage on Ru₂/MoS₂.

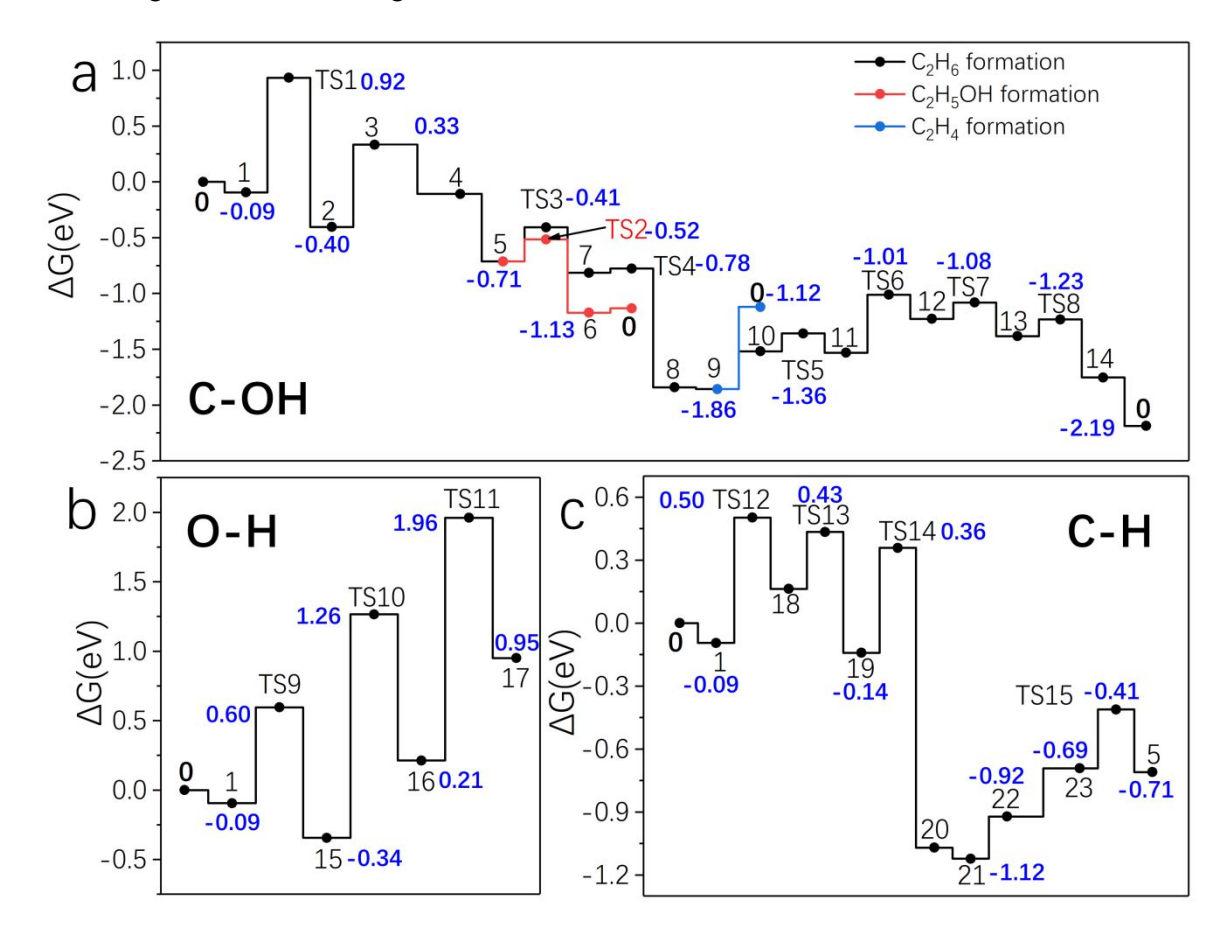


Figure 3. Free energy profiles of EG DODH on Ru₂/MoS₂ at 423 K. The partial pressures of all gas phase molecules are set to be 1 bar. The Ru₂ notation is omitted in the energy diagram for brevity. Each elementary step is also described in Table S3.

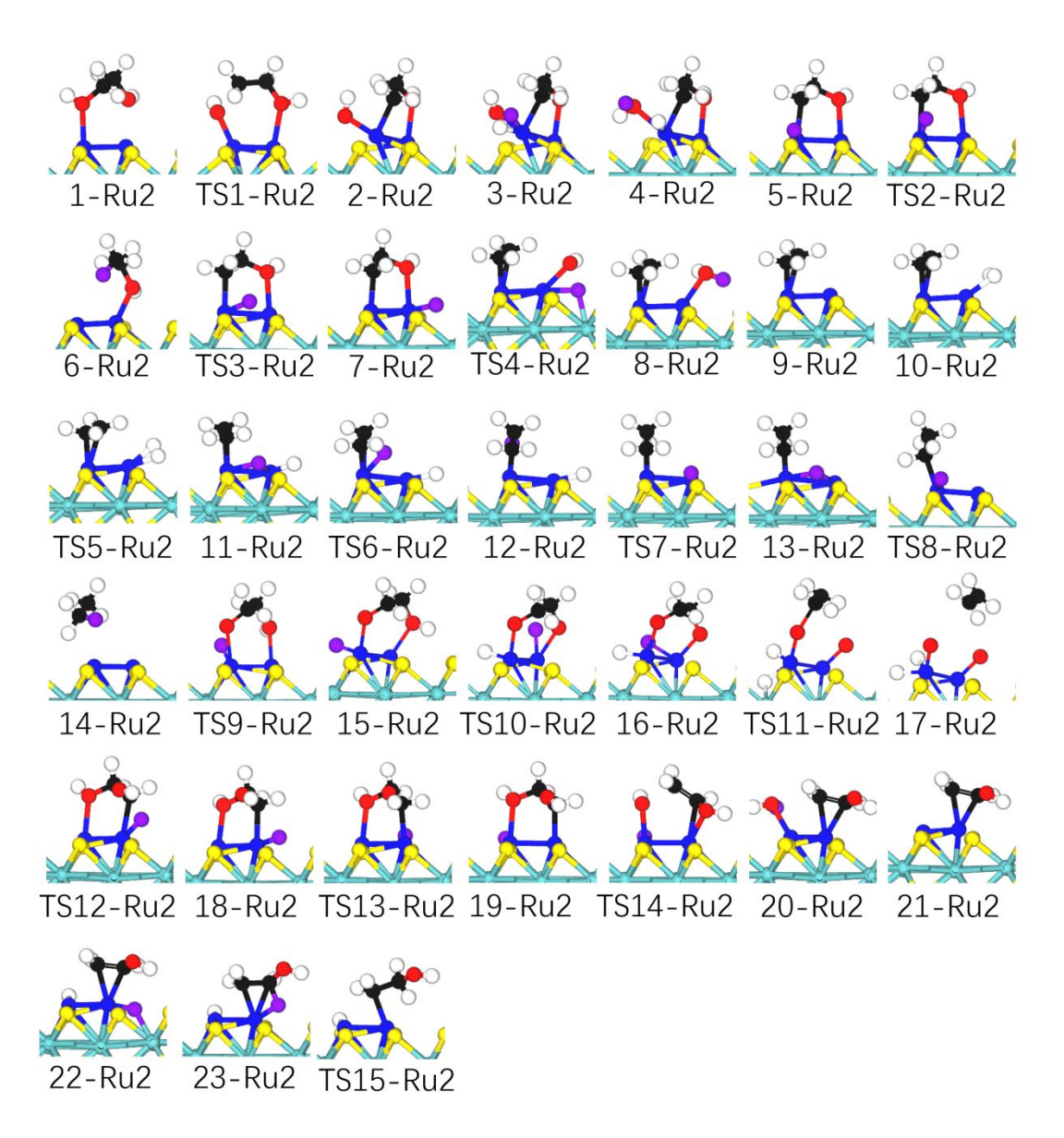


Figure 4. Structures of intermediate and transition states for the energy profiles in Figure 3.

3.3 DODH of EG on Ir₂/MoS₂

Next, we investigated the DODH reaction of EG on Ir_2/MoS_2 . The direct cleavage of the C-OH bond needs to overcome a high barrier of 1.36 eV (1- $Ir_2\rightarrow 2$ - Ir_2), as displayed in Figure 5 and 6. The dissociative chemisorption of a H_2 molecule on 2- Ir_2 is endergonic by 0.42 eV. Next the formation (3- $Ir_2\rightarrow 4$ - Ir_2) and desorption (4- $Ir_2\rightarrow 5$ - Ir_2) of H_2O can occur readily. The atomic hydrogen of 5- Ir_2 can migrate to another Ir atom to adopt a more energetically favorable configuration (16- Ir_2). Similar to the case of Ru_2/MoS_2 , the presence of H_2O does not facilitate the C-OH bond cleavage (Figure S4). The first and second O-H bond cleavage can readily occur on Ir_2/MoS_2 (1- $Ir_2\rightarrow 6$ - Ir_2 and 6- $Ir_2\rightarrow 7$ - Ir_2).

However, the ethylene extrusion is highly unfavorable, similar to the case of Ru₂/MoS₂. Since the direct C-OH cleavage or the ethylene extrusion process does not allow for the DODH of EG due to high energy barriers, we also investigated the C-H activation mechanism on Ir₂/MoS₂.

C-H activation of EG on Ir₂/MoS₂ has a barrier of 0.78 eV and is endergonic by 0.11 eV. The transition state energies of the ensuing hydrogen migration (9-Ir₂→10-Ir₂) and C-OH bond cleavage (10-Ir₂→11-Ir₂) are lower than those of the C-H activation. The C-OH bond cleavage is accompanied by the formation of H₂O. Since the energy profile of the first O-H bond cleavage step, which is energetically downhill by 0.15 eV, is kinetically more favorable than the C-H activation, the effective barrier of the C-OH cleavage through the C-H activation mechanism is increased by 0.15 eV, being 0.93 eV. Next, a H₂ molecule is chemisorbed to 12-Ir₂ so that the reaction can proceed. The ensuing hydrogen migration (13-Ir₂→14-Ir₂) and addition (14-Ir₂→15-Ir₂) steps, as well as the CH₂CH₂OH migration step (15-Ir₂→16-Ir₂) possess relatively low barriers. 16-Ir₂ can be hydrogenated to form an ethanol molecule or further deoxygenated by undergoing facile H migration (16-Ir₂→18-Ir₂) and C-OH scission steps (18-Ir₂→19-Ir₂). The dissociation of the ethanol O-H bond is energetically downhill by 0.34 eV (17-Ir₂→25-Ir₂), rendering the effective barrier of ethanol C-OH bond cleavage to be 0.87 eV (Figure S3). Upon the desorption of the H₂O molecule (19-Ir₂→20-Ir₂), the catalytic cycle of the EG DODH process is completed on Ir₂/MoS₂. The desorption of C₂H₄ (20-Ir₂→0-Ir₂) is unfavorable while the hydrogenation of it (21-Ir₂→24-Ir₂) only requires overcoming an effective barrier of 0.69 eV.

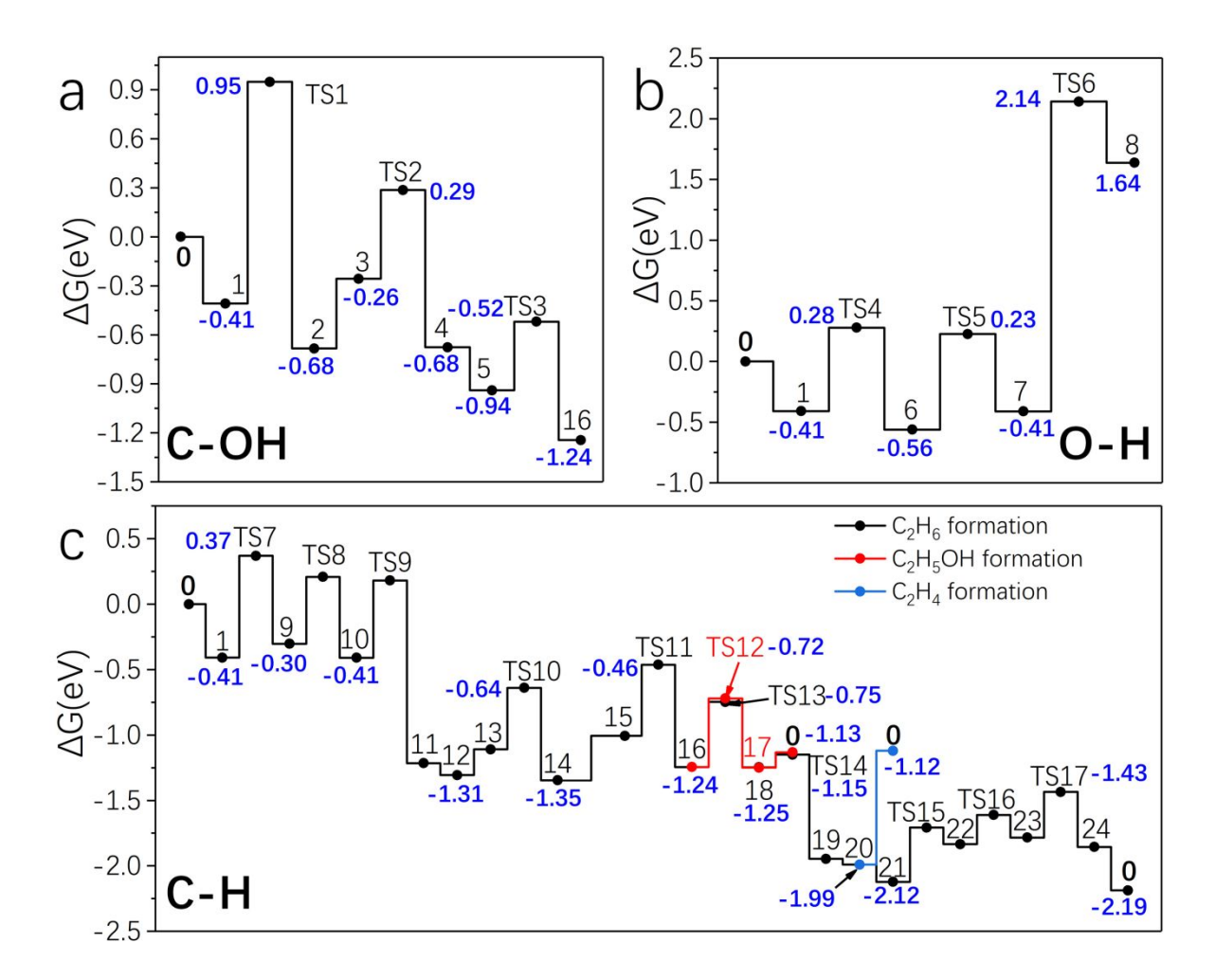


Figure 5. Free energy profiles of EG DODH on Ir₂/MoS₂ at 423K. The partial pressures of all gas phase molecules are set to be 1 bar. The Ir₂ notation is omitted in the energy diagram for brevity. Each elementary step is also described in Table S4.

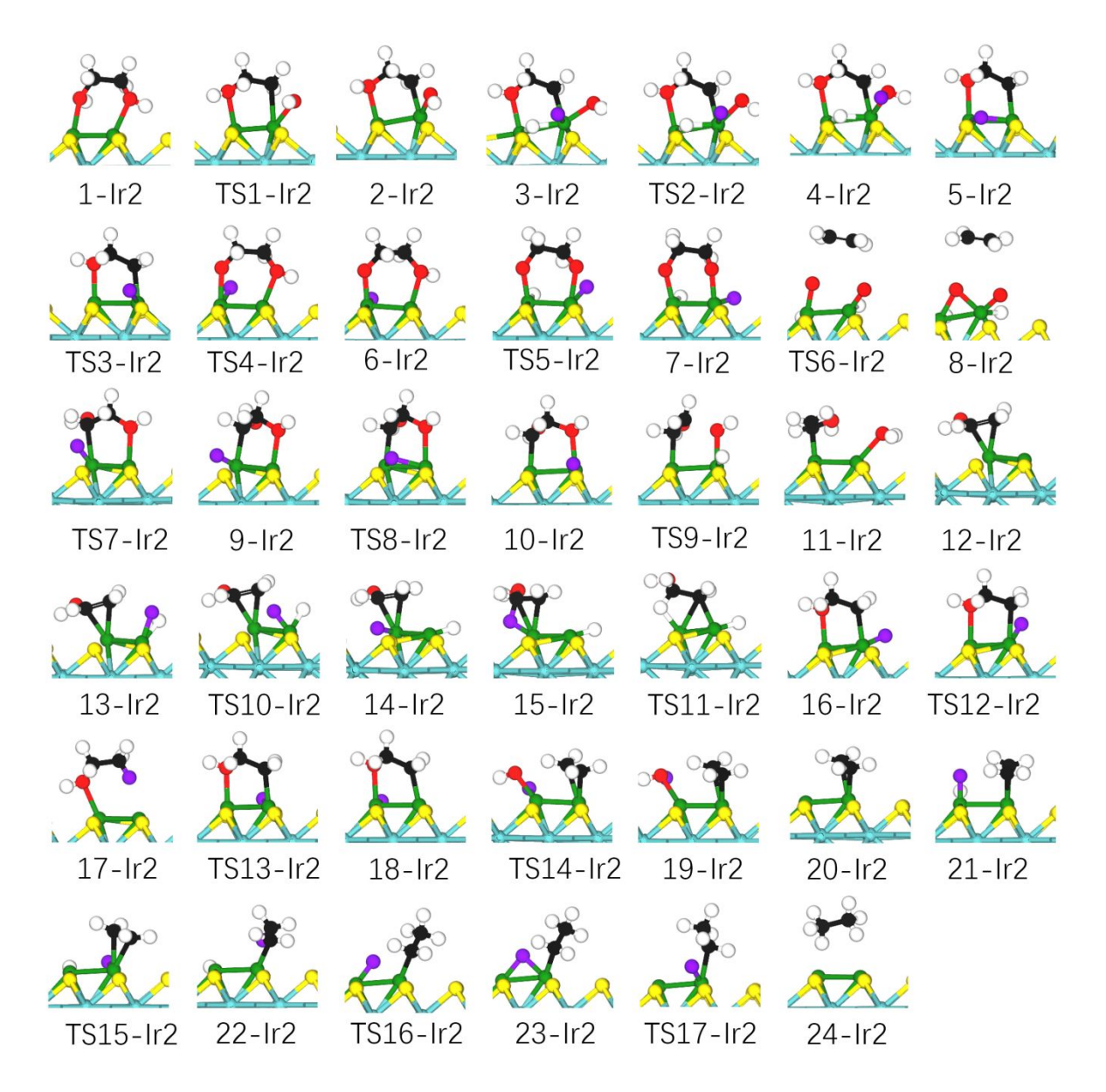


Figure 6. Structures of intermediate and transition states for the energy profiles in Figure 5.

Along the C-H activation pathways, we found that the effective barriers of the first C-OH cleavage on Ru₂/MoS₂ and Ir₂/MoS₂ are noticeable lower than those on their single-atom counterparts. Probably, this originates from the C-H activation and C-OH cleavage occurring on different metal atoms for the atom-pair catalysts; thus, avoiding the need to reorient the reaction intermediates significantly as required for the single-atom catalysts after C-H activation (6-Ru₁ and 6-Ir₁) so that the C-OH bond cleavage can occur.

3.4 DODH of EG on Ru₃/MoS₂ and Ir₃/MoS₂

After establishing the energy profiles of MoS₂-supported atom-pair catalysts for the DODH of EG, we examined the feasibility of Ru₃/MoS₂ and Ir₃/MoS₂ as DODH catalysts. In other words, we studied if the activity is unique to atom-pair catalysts or if other small metal clusters on MoS₂ can also catalyze the DODH. The cleavage of the EG C-OH bond on Ru₃/MoS₂ requires overcoming a barrier of 1.18 eV (see Figures 7 and S2), as compared to 0.77 eV for the O-H scission and 1.01 eV for C-H scission. As shown in Figure 7b, the second O-H cleavage and the extrusion of ethylene requires overcoming high energy barriers and are both endergonic. Along the C-H activation pathway, the transition state energy of the C-OH cleavage (TS7-Ru₃) is 0.02 eV higher than that of the C-H activation (TS6-Ru₃). Unlike Ru₂/MoS₂ or Ir₂/MoS₂, the C-OH bond cleavage is not concomitant with the formation of H₂O for the case of Ru₃/MoS₂, probably because OH and H are situated at different Ru atoms for 9-Ru₃. The association of OH and H (9-Ru₃ \rightarrow 10-Ru₃) has a barrier of 0.87 eV. After the chemisorption of a H₂ molecule, the migration and addition of a H atom to ethenol (11-Ru₃ \rightarrow 14-Ru₃), a CH₂CH₂OH intermediate is formed. Both the removal of the second OH (14-Ru₃ → 16-Ru₃) and the H addition to the CH₂CH₂OH intermediate (14-Ru₃ → 15-Ru₃) can readily occur, with the latter process being preferred. We mention here that while the dissociation of the ethanol O-H bond is exergonic by 0.44 eV, the energy of 25-Ru₃ lies above that of the free site 0-Ru₃ (Figure S3). Therefore, the effective barrier of the ethanol C-OH bond cleavage is not increased by the O-H bond dissociation. Two H migration steps (16-Ru₃ \rightarrow 17-Ru₃ and 17-Ru₃ \rightarrow 18-Ru₃) occur before the association of H and OH. The formation of the second H_2O (18-Ru₃ \rightarrow 19-Ru₃) involves overcoming a 0.74 eV free energy barrier. Finally, 20-Ru₃ → 24-Ru₃ corresponds to the ethylene hydrogenation process, whose effective free energy barrier was calculated to be 0.79 eV.

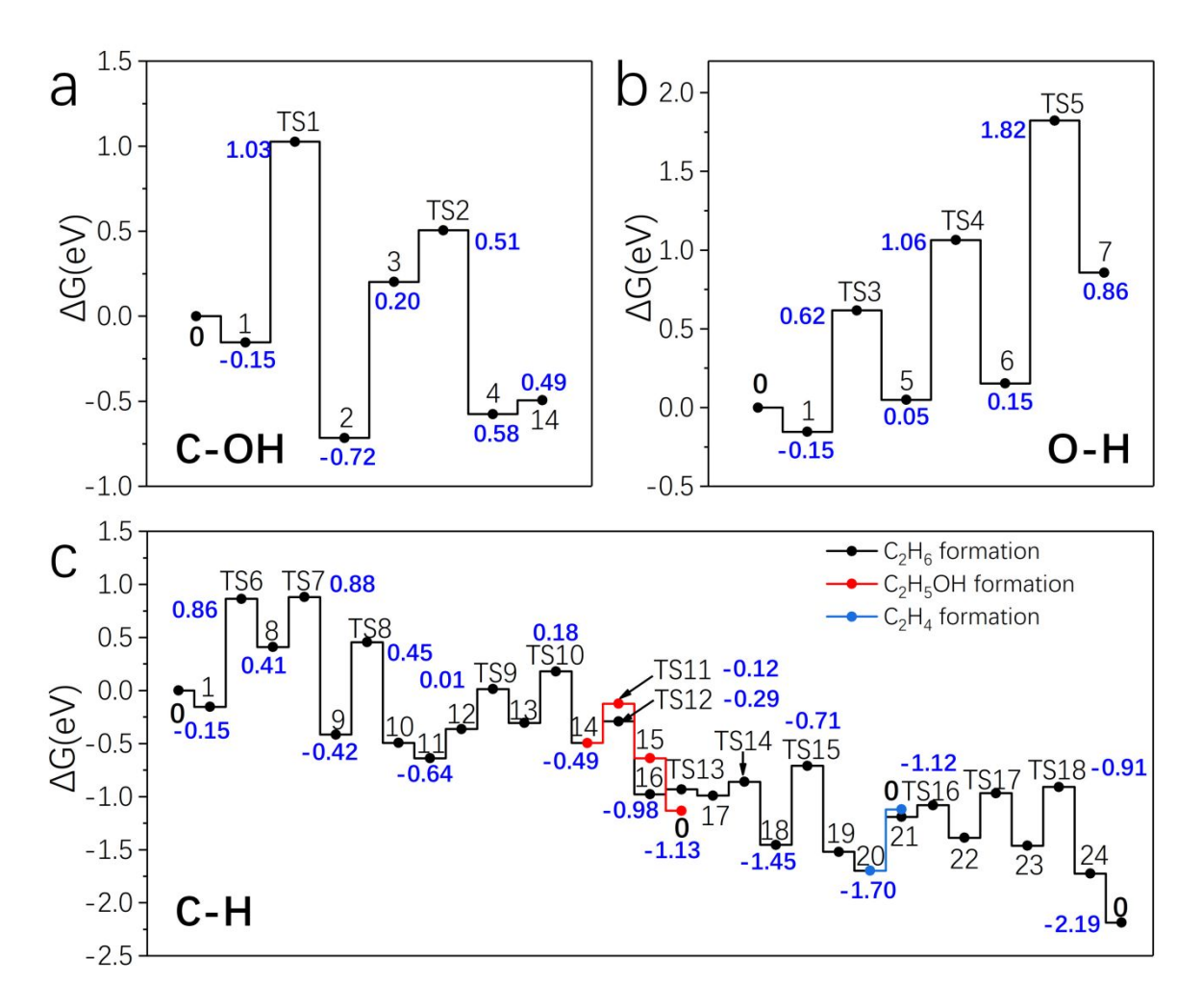


Figure 7. Free energy profiles of EG DODH on Ru₃/MoS₂ at 423 K. The partial pressures of all gas phase molecules are set to be 1 bar. The structures of each intermediate and transition state are presented in Figure S5. The Ru₃ notation is omitted in the energy diagram for brevity. Each elementary step is also described in Table S5.

The reaction mechanism of the EG DODH was also examined on Ir_3/MoS_2 (see Figures 8 and S3). The free energy barriers of the C-OH and O-H bond cleavage on Ir_3/MoS_2 are 0.50 and 0.06 eV higher than those of the C-H activation, respectively. The removal of the first OH group (8- $Ir_3\rightarrow 9$ - Ir_3) and the H_2O formation (9- $Ir_3\rightarrow 10$ - Ir_3) are facile after the C-H activation step. After the dissociative chemisorption of H_2 on 11- Ir_3 , one H atom can migrate to the Ir atom where CH_2CHOH is adsorbed. The hydrogen addition on the α -carbon of CH_2CHOH (13- $Ir_3\rightarrow 14$ - Ir_3) has a free energy barrier of 0.72 eV, followed by facile removal of the second OH (14- $Ir_3\rightarrow 16$ - Ir_3) or formation of ethanol (14- $Ir_3\rightarrow 15$ - Ir_3). Considering that the ethanol O-H bond dissociation is exergonic by 0.32 eV (Figure S3), the effective barrier of the 15- $Ir_3\rightarrow 14$ - $Ir_3\rightarrow 16$ - Ir_3 process was calculated to be 1.08 eV, corresponding to

the C-OH bond cleavage of ethanol. The formation of the second H_2O (16-Ir₃ \rightarrow 17-Ir₃) needs to overcome a free energy barrier of 0.84 eV. Finally, the formed H_2O desorbs readily and C_2H_4 can be hydrogenated with an effective barrier of 0.70 eV.

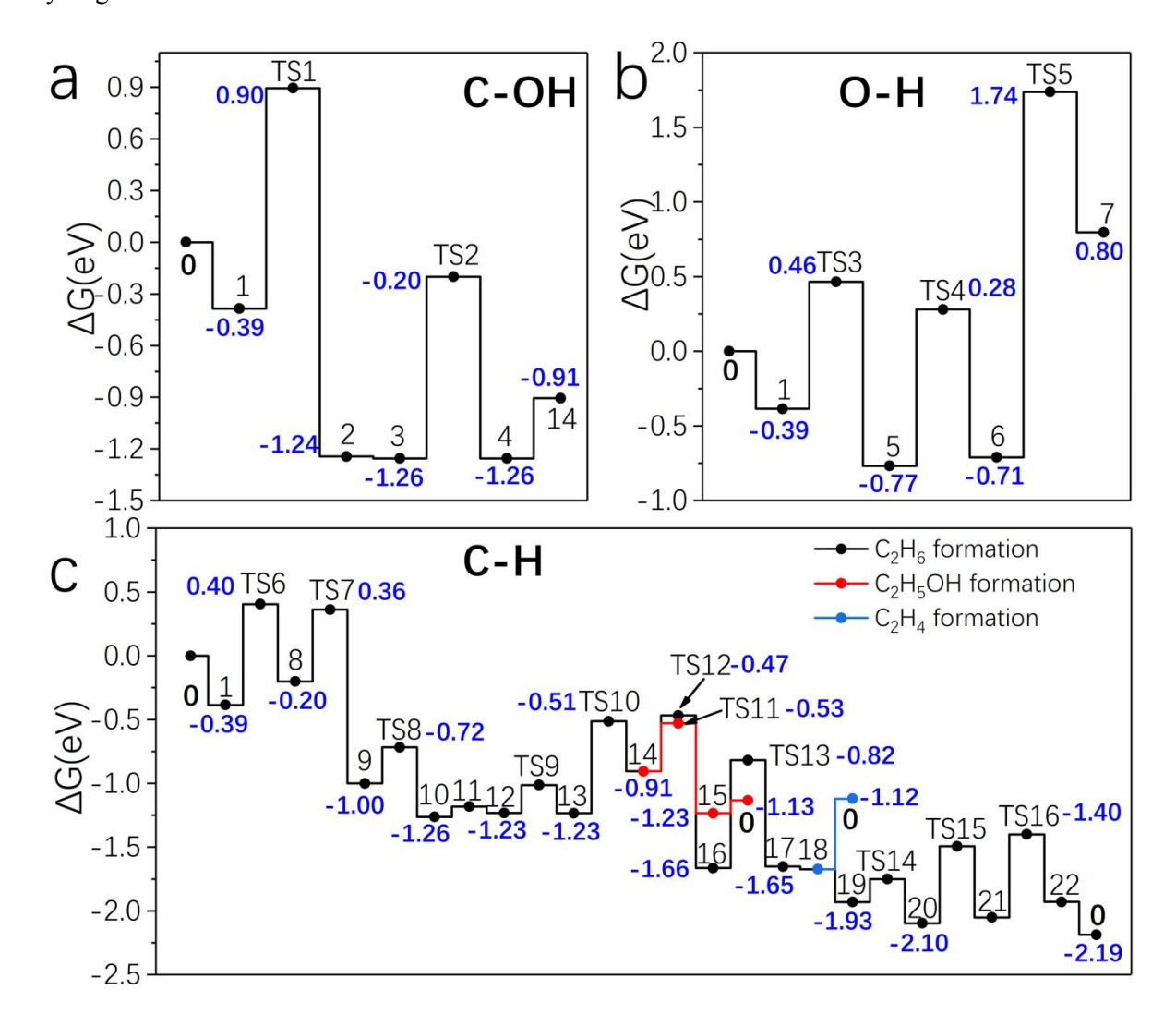


Figure 8. Free energy profiles of EG DODH on Ir₃/MoS₂ at 423 K. The partial pressures of all gas phase molecules are set to be 1 bar. The structures of each intermediate and transition state are presented in Figure S6. The Ir₃ notation is omitted in the energy diagram for brevity. Each elementary step is also described in Table S6.

After presenting the energy profiles of the DODH of EG, we compared the effective free energy barriers of the first C-OH cleavage via the direct mechanism and the C-H activation mechanism. It is found that the abstraction of an H atom consistently lowers the barrier of the C-OH cleavage, as displayed in Figure 9, where we compared the effective barriers of the two mechanisms over MoS₂-

supported Ru₁-Ru₃, Ir₁-Ir₃, Pt₂ and Rh₂ (see Figure S7 for the free energy profiles of the EG C-H and C-OH bond dissociation on Pt₂/MoS₂ and Rh₂/MoS₂). This trend is also consistent with a previous study showing that a dehydrogenation step facilitates the C-OH bond cleavage on the neighboring carbon during the hydrodeoxygenation of propanoic acid on a Pd(111) surface.⁴⁸

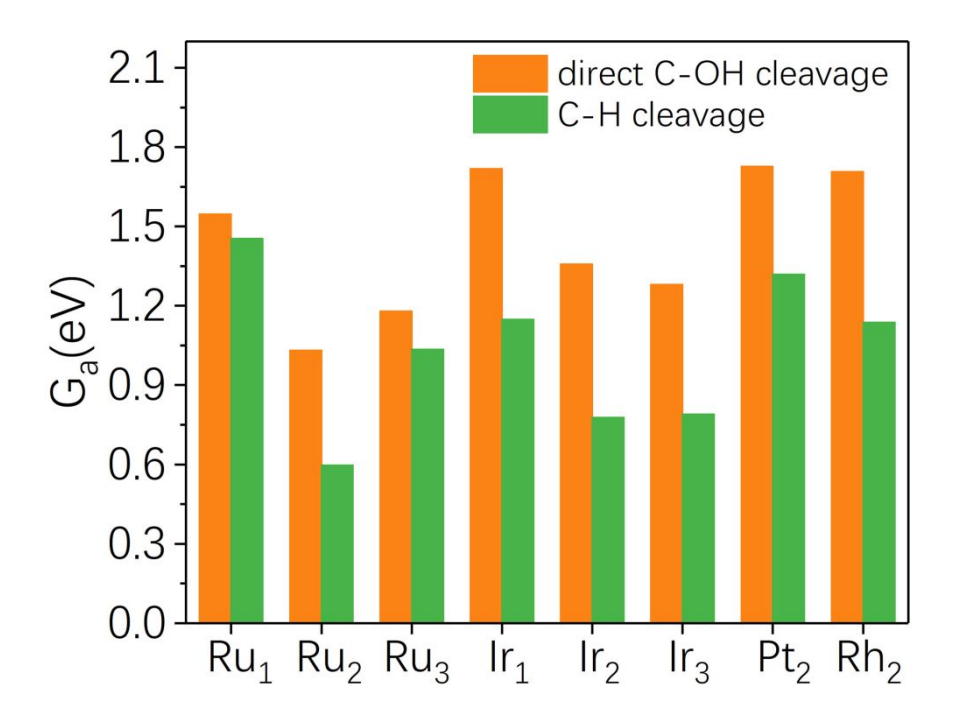


Figure 9. Comparison of the effective activation free energies for the C-OH bond cleavage through the direct bond-cleavage mechanism and the C-H activation mechanism.

Given that we have shown that Ru₂/MoS₂, Ir₂/MoS₂, Ru₃/MoS₂ and Ir₃/MoS₂ have favorable energy profiles for the DODH of EG, it is necessary to examine the stability of the proposed catalysts. While the calculated formation energies of Ru₂/MoS₂ and Ir₂/MoS₂ are slightly positive with respective to the bulk metals, the migration of Ru or Ir to a neighboring site are thermodynamically unfavorable and need to overcome high barriers (Table 1, also see Figure S8 for the configurations for the initial and final states of atom migration). A high hopping barrier of the metal atoms was used previously to evaluate the stability of single-atom catalyst.^{34,49} Here, we found that at 473 K (50 K higher than typical DODH condition), the hopping rate of Ir was calculated to be 1.81×10-9/s for Ir₂/MoS₂, suggesting that the aggregation of Ir is prevented. Table 1 illustrates that Ru₂/MoS₂ and Ru₃/MoS₂ are also stable under DODH reaction conditions, considering that the Ru migration barriers are even higher than those of Ir₂/MoS₂. While the Ir migration barrier of Ir₃/MoS₂ is relatively low (1.44 eV), it is energetically uphill

and the formation energy of Ir₃/MoS₂ is negative. Therefore, the four catalysts are all stable under practical reaction conditions. To further demonstrate the importance of sulfur vacancies on MoS₂, we show in Figure S9 that metal cluster dissociation and Ru/Ir atom diffusion of pristine MoS₂-supported Ru₂ and Ir₂ have low barriers, suggesting that sintering of Ru/Ir atoms can occur readily on pristine MoS₂.

Table 1. Calculated formation energy (in eV) per metal atom (E_f , the reference states are MoS_2 with two or three S vacancies and bulk metals), free energy barrier of metal atom migration (G_a) and free energy change of the migration process (ΔG).

	$E_{\rm f}$	Ga	ΔG
Ru ₂ /MoS ₂	0.58	2.24	1.91
Ir ₂ /MoS ₂	0.37	2.04	2.01
Ru ₃ /MoS ₂	0.00	4.17	3.23
Ir ₃ /MoS ₂	-0.12	1.44	0.41

3.5 Microkinetic modelling of EG DODH on Ru₂/MoS₂, Ir₂/MoS₂, Ru₃/MoS₂ and Ir₃/MoS₂

Finally, microkinetic models were developed to understand the DODH reaction kinetics (see Table S7-S12 for the rate constants of each elementary step). The fugacity and gas phase partial pressure of EG were estimated using Raoul's law, the three-parameter Antoine equation $(\log_{10}(P^{SAT}) = A - (B/(T + C))$, A=4.97012, B=1914.951, C=-84.996, PSAT is the partial pressure in bar, T is the temperature in K),⁵⁰ and the assumption of a pure liquid EG phase. The fugacities/partial pressures of EG are calculated at 353, 373 and 423K to be 6.94×10^{-3} , 0.021 and 0.20 bar, respectively.

In the following, if the partial pressures/fugacities of the fluid phase molecules are not specified, they are set to 1 bar in the microkinetic models (MKMs). Since the desorption of ethylene is energetically uphill by more than 0.5 eV at 423 K and the hydrogenation of it can readily occur in the four cases, our MKMs suggest that ethylene is hydrogenated to ethane. Thus, we set the ethane partial pressure to 1 bar and the ethylene partial pressure to around 10⁻¹⁰ bar such that the production rate of ethylene is 0. Such a low concentration of ethylene can be reached quickly during the initial stages of

the DODH reaction.

The favorable energy profile of the EG DODH over Ru₂/MoS₂ allows the reaction to be operated at a lower temperature than the typical DODH reaction temperature of 423 K. Specifically, at 353 K and fluid phase fugacities/partial pressures of EG: 6.94×10⁻³ bar, C₂H₅OH: 6.94×10⁻³ bar, C₂H₄: 1×10⁻³ ¹⁰ bar, H₂: 1 bar, H₂O: 1 bar, and C₂H₆: 1 bar (the reaction order with respect to ethane and water is zero, i.e., the specific values have no influence on the rate), the MKM of the DODH reaction over Ru₂/MoS₂ predicts a turnover frequency (TOF) of EG consumption of 4.02/s, with the formation rates of ethanol and ethane of 3.87/s and 0.15/s, respectively. In other words, ethanol is the major product at the initial stage of the reaction and only after most of the EG is consumed, is ethanol converted to ethane. The reaction mainly proceeds through a C-H activation mechanism while the contribution of the direct C-OH cleavage pathway is negligible (1.9×10⁻⁶/s). We also set the fugacity/partial pressure of EG to a low value of 1×10⁻⁶ bar (called low EG fugacity case hereafter, here the ethanol fugacity remains at 6.94×10⁻¹ ³ bar) to simulate the case when EG reaches ~100% conversion to ethanol. Under these conditions, the consumption rates of ethanol and EG are calculated to be 3.73/s and 0.72/s, respectively. The apparent activation energies are 0.90 and 0.88 eV for the high (EG fugacity is 6.94×10⁻³ bar) and low EG fugacity cases, respectively (see Figure 10a). Table S13 displays the degrees of rate control (DRC)⁵¹ for the most rate-controlling steps at high and low EG fugacity conditions, which were identified to be 1-Ru₂-18- $\mathbf{Ru_2}$ (the first C-H activation step of EG, DRC = 0.84) and $\mathbf{11}$ - $\mathbf{Ru_2} \rightarrow \mathbf{12}$ - $\mathbf{Ru_2}$ (the first hydrogenation step of ethylene, DRC = 0.82) at high and low EG fugacity conditions, respectively. At 353 K and typical H₂ (1-10 bar) and EG (6.94×10⁻⁴-6.94×10⁻³ bar) fugacities, we predict H₂ and EG reaction orders of 0.01 and 0, respectively. We note here that a Ru-based homogeneous DODH catalyst $([Cp*Ru(CO)_2]_2, Cp* = 1,2,3,4,5$ -pentamethylcyclopentadienyl) has previously been proposed experimentally; however, the TOF for the DODH of 1,2-hexanediol catalyzed by the Ru-based catalyst is only 3.5×10^{-4} /s and the activity for other substrates is even lower.⁵²

Next, we developed an microkinetic model for the reaction on Ir_2/MoS_2 at 373 K (a slightly higher temperature than that of Ru_2/MoS_2 is used such that the TOF is over 1/s) and partial pressures of EG, ethanol, and ethane set to 0.021, 0.020 bar and 1×10^{-10} bar such that the formation rates of ethanol and ethylene are 0. We note that if the partial pressure of ethanol is set to a value higher than 0.020 bar ethanol is consumed. Under such conditions, the TOF of EG consumption is 1.53/s. With partial pressures of EG and ethanol being set to 10^{-6} and 0.02 bar, respectively, the formation rate of ethane

was calculated to be 10.97/s. The rate-determining step at high and low EG fugacities were found to be $1-Ir_2\rightarrow 9-Ir_2$ (the first C-H activation step of EG) and $17-Ir_2\rightarrow 16-Ir_2$ (the dehydrogenation of step ethanol), respectively, and the corresponding DRCs are 0.75 and 0.71 (Table S13). The apparent activation energy at high and low EG fugacities were calculated to be 0.95 and 0.84 eV, respectively (Figure 10b). We also found that the reaction orders of EG (0.0021-0.021 bar) and H₂ (1-10 bar) are 0 for the reaction on Ir_2/MoS_2 .

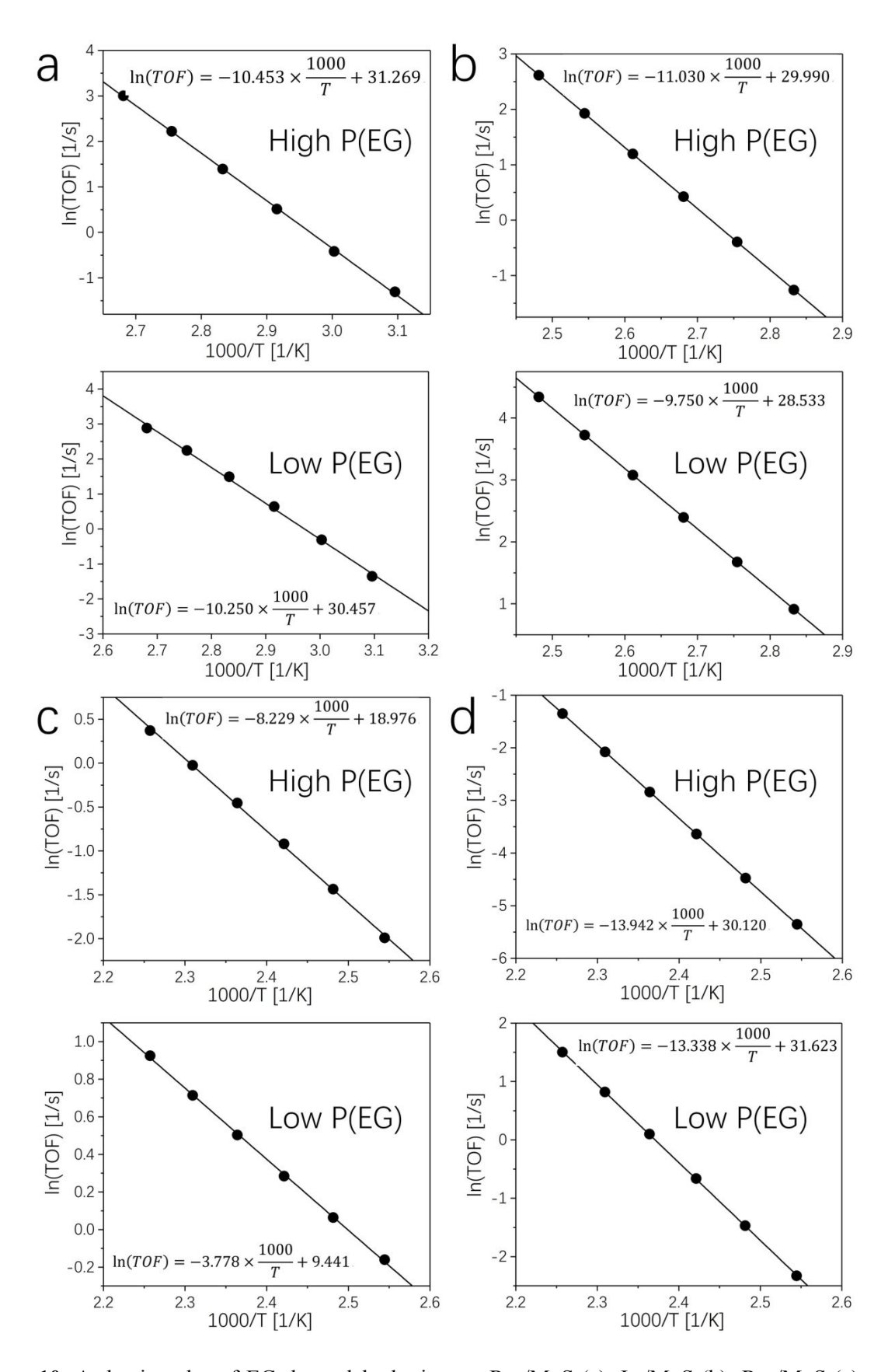


Figure 10. Arrhenius plot of EG deoxydehydration on $Ru_2/MoS_2(a)$, $Ir_2/MoS_2(b)$, $Ru_3/MoS_2(c)$ and $Ir_3/MoS_2(d)$ at high $(Ru_2/MoS_2, 6.94 \times 10^{-3} \text{ bar}; Ir_2/MoS_2, 0.021 \text{ bar}; Ru_3/MoS_2 \text{ and } Ir_3/MoS_2, 0.20 \text{ bar})$

and low (10^{-6} bar in all cases) fugacities/partial pressures of EG. The temperature ranges for the calculation over Ru₂/MoS₂ and Ir₂/MoS₂ are 323-373 K and 353-403 K, respectively. The TOFs of both Ru₃/MoS₂ and Ir₃/MoS₂ are calculated in the temperature range of 393-443 K.

For Ru₃/MoS₂, our MKM was performed at 423 K with the partial pressure of EG set to be 0.20 bar. We set the ethylene partial pressure to be 8×10^{-9} bar so that the production rate of ethylene is 0. We also found that the conversion rate of EG to ethanol is 0 with an ethanol partial pressure of 0.20 bar. Compared with the case of Ru₂/MoS₂, the less favorable formation of ethanol for Ru₃/MoS₂ is due to TS11-Ru₃ being energetically higher than TS12-Ru₃. With the setup of fugacity/partial pressures so that the conversion rates to ethanol and ethylene are 0, we found that the TOF of ethane production is 0.63/s at 423 K. By increasing the H₂ partial pressure from 1 bar to 10 bar, the TOF is increased to 1.96/s, accompanied with a decrease of the 2-Ru₃ surface coverage from 0.75 to 0.23. We obtained a reaction order of 0.48 for H₂ (1-10 bar). A high barrier of the step 1-Ru₃ \rightarrow 2-Ru₃ (the direct C-OH bond cleavage, DRC=-0.79 in Table S13) and a low barrier of the step 3-Ru₃→4-Ru₃ (the association of H and OH, DRC=0.74) is favorable for the reaction kinetics at high EG fugacity. Also, the reaction kinetics is largely affected by the 1-Ru₃→8-Ru₃ (the first C-H activation step of EG) and 8-Ru₃→9-Ru₃ (a H migration step), whose DRCs are calculated to be 0.37 and 0.59, respectively. At low EG fugacity (C₂H₅OH, 0.2 bar; C₂H₄, 8×10⁻¹¹ bar), the formation rate of ethane is calculated to be 1.65/s. The rate-determining step is found to be 15-Ru₃ $\rightarrow 14$ -Ru₃ (the dehydrogenation of ethanol) with a DRC of 0.98 (Table S13). The apparent activation energy at high and low EG fugacities were calculated to be 0.71 and 0.33 eV, respectively (Figure 10c).

On Ir₃/MoS₂, we found that the TOF of EG consumption is 0.058/s at 423 K (EG, 0.20 bar; C₂H₅OH, 0.20 bar; C₂H₄, 1×10⁻¹⁰ bar), with the C₂H₅OH and C₂H₆ formation rate being 0.049 and 0.009/s, respectively. The relatively low TOF, as compared with the case of Ru₂, Ru₃, and Ir₃, can be attributed to the fact that **TS3-Ir**₃ is only 0.06 eV energetically higher than **TS6-Ir**₃ while **5-Ir**₃ is 0.58 eV lower than **8-Ir**₃ (Figure 8). This suggests that the O-H cleavage of EG is competitive with the C-H cleavage and the formation of **5-Ir**₃ increases the effective barrier of the C-H activation from 0.79 eV to 1.17 eV (assuming that **5-Ir**₃ is the initial state). When ethanol is formed, we found a relatively high ethanol to ethane TOF of 1.10/s. Here, we also considered the cleavage of ethanol O-H bond (Figure S3), therefore, the effective barrier of the ethanol C-OH bond cleavage was calculated to be 1.07 eV. The rate-

determining step of the DODH reaction on Ir_3/MoS_2 at the high and low EG fugacities were identified to be **1-Ir₃** \rightarrow **8-Ir₃** (the activation of EG C-H bond, DRC= 0.75 in Table S13) and **14-Ir₃** \rightarrow **16-Ir₃** (the second C-OH bond cleavage, DRC= 0.84), whose apparent activation energies were calculated to be 1.20 and 1.15 eV, respectively (see Figure 10d).

To better understand the role of MoS₂ support, we next examined the DODH of EG on Ru(0001), Ir(111), and anatase TiO₂(101)-supported Ru₂ and Ir₂, as shown in the Supporting discussions of the SI and Figures S10-S19. We found that the Ru(0001) and Ir(111) surfaces are covered by hydrogen atoms under reaction conditions and the effective barriers of the C-OH cleavage along the C-H activation pathway are relatively high, making Ru(0001) and Ir(111) inactive for the DODH of EG. The exergonic adsorption of H₂ (greater than that of EG) on Ru₂/TiO₂(101) and Ir₂/TiO₂(101) is partially responsible for the high effective barriers of the DODH processes. Overall, the C-H activation pathways are preferred over the direct C-OH cleavage pathways, which is consistent with the conclusion we obtained for the MoS₂-supported metal clusters (Figure 9). The density of states of Ru atoms for Ru₂/TiO₂(101) and Ru(0001) are significantly different to that of Ru₂/MoS₂(Figure S20), and this is also true for the Ir₂ counterparts. In particular, noticeable spin-polarization is observed for Ru₂/MoS₂ and Ir₂/MoS₂ near the Fermi level, which is likely responsible for the high catalytic activities.

Thus, we have shown that Ru₂/MoS₂, Ir₂/MoS₂ and Ru₃/MoS₂ exhibit a high activity for the DODH of EG while the activity of Ir₃/MoS₂ is only moderately high and that this high activity is a result of the interaction of the metal sites with the MoS₂ support. The calculated TOF of EG consumption on at 443K on Ir₃/MoS₂ was calculated to be 0.26/s, which is comparable with the experimental TOF (0.083/s)⁵ of the cis-1,4-anhydroerythritol DODH reaction on a ReO_x–Pd/CeO₂ catalyst or the computational value of 0.42/s.¹⁴ The alkene extrusion was identified to be the rate-determining step with an effective barrier of 1.11 eV for the reaction on ReO_x–Pd/CeO₂, where the DODH process on ReO_x is affected by the Pd cluster neighboring it.¹⁴ In another case of ReO_x/CeO₂, for which the Pd co-catalyst is distant from the ReO_x catalytic center and only serves the role of H₂ dissociation, the rate-determining step of the reaction was found to be the first O-H cleavage step with an effective barrier of 1.18 eV and a calculated TOF of 4.33×10⁻³/s.¹⁴ In our present study, the MoS₂-supported Ru₂, Ir₂ and Ru₃ catalyst allows the DODH reaction to occur with significantly higher TOF than the conventional heterogeneous DODH catalyst occurring on a MO_x catalytic center. The improved activity is attributed to the fact that Ru⁵³ or Ir⁵⁴ can activate the C-H bond readily and that the preliminary C-H activation step makes the ensuing

C-OH readily occur. Also, the exergonic chemisorption of EG on transition metal sites contrasts the case of the endergonic physisorption of cis-1,4-anhydroerythritol on the ReO_x site that increases the effective barrier for the O-H bond cleavage. Moreover, the ability of activating H₂ by Ru or Ir atomic clusters avoids the need of a co-catalyst for H₂ activation, as in the case of ReO_x-Pd/CeO₂. Considering that the conversion rate of ethanol to ethane is over 1/s in all cases, the proposed DODH catalysts are also highly active as hydrodeoxygenation catalyst for the removal of alcohol OH groups. Finally, we also compared the activity of the proposed MoS₂-supported DODH with conventional homogeneous DODH catalysts. The effective barrier of a homogeneous methyltrioxorhenium (CH₃ReO₃) catalyzed DODH of 3-ene-1,2-diol was calculated to be 1.05 eV.⁵⁵ Therefore, the activities of the proposed heterogeneous catalysts in the present study are most likely comparable with conventional homogeneous catalyst.

4. Conclusions

We performed a first principles study of the ethylene glycol deoxydehydration reaction on MoS₂supported Ru and Ir atoms. Our calculations suggest that while the activities of Ru₁/MoS₂ and Ir₁/MoS₂ are relatively low, Ru₂/MoS₂, Ir₂/MoS₂, and Ru₃/MoS₂ exhibit high activities for the conversion of ethylene glycol to ethanol and ethanol to ethane, with a calculated TOF of over 1/s at typical DODH reaction condition of 423 K or even lower temperatures of 353 K. The higher activity of the reactions on MoS₂-supported atoms underscores the synergistic effect between neighboring Ru or Ir atoms and to the MoS₂ support. The activity of the less active Ir₃/MoS₂ is comparable to that of conventional DODH catalysts with a MO_x species as the active center. Importantly, our calculations suggest that an initial C-H activation step makes the C-OH bond cleavage on the neighboring carbon facile, a mechanism that was also identified on Pt₂/MoS₂ and Rh₂/MoS₂. Thus, the improved activity of MoS₂supported Ru/Ir catalysts relative to conventional DODH catalysts can be attributed to EG adsorption being exergonic on transition metal sites (while it is endergonic on MO_x sites), effectively lowering the overall barrier, and C-H activation reducing the energy barrier of the subsequent C-OH cleavage process. To better understand the role of the MoS₂ support, we examined the DODH of EG on Ru(0001), Ir(111), anatase TiO₂(101)-supported Ru₂ and Ir₂, which are all essentially inactive for the DODH of EG. The effective barrier for the DODH of EG on these four surfaces are 1.46 eV (Ru₂/TiO₂) or higher. This highlights the role of the MoS₂ support, which is probably related to the unique density of states for Ru

or Ir atoms of MoS₂-supported Ru and Ir clusters. Apart from being a DODH catalyst, the proposed MoS₂-supported catalysts are also highly active as hydrodeoxygenation catalyst for the removal of alcohol OH groups; and we suggest a new mechanism for the DODH reaction and provide a meaningful guideline for the design of highly active DODH catalysts.

Author information

Corresponding Author

*E-mail for A.H.: heyden@cec.sc.edu.

Notes

The authors declare no competing financial interest.

Associated content

Supporting Information

Adsorption free energy of EG and H₂, description of each elementary step, free energy profiles of the ethanol O-H bond dissociation, relative stability of MoS₂-supported Ru₂, Ru₃, Ir₂, Ir₃ as well as the corresponding supported single-atoms, different adsorption configurations of ethylene glycol on MoS₂-supported metal clusters, the structures of intermediate and transition states for the reactions on Ru₃/MoS₂ and Ir₃/MoS₂, free energy profiles of the C-OH cleavage for EG through the direct pathway and the C-H activation pathway on Pt₂/MoS₂ and Rh₂/MoS₂, initial and final states of Ru and Ir atom migration, initial and final states of Ru migration on Ru₂/MoS₂ and Ru₃/MoS₂, as well as Ir migration on Ir₂/MoS₂ and Ir₃/MoS₂, free energy change for the Ru/Ir atom diffusion of pristine MoS₂-supported Ru₂ and Ir₂, DODH of EG on Ru(0001)/Ir(111), DODH of EG on Ru₂/TiO₂(101) and Ir₂/TiO₂(101), density of states for the Ru/Ir atoms of MoS₂- and TiO₂-supported Ru₂/Ir₂, as well as two surface atoms of Ru(0001) and Ir(111), details of the microkinetic model and calculated values for the degree of rate control, coordinate files for all the intermediate and transition states.

Acknowledgments

We gratefully acknowledge financial support from the National Science Foundation (OIA-1632824). The research was performed using computing resources from EMSL (Ringgold ID 130367, Grant Proposal 49246), a DOE Office of Science User Facility sponsored by the Office of Biological

and Environmental Research and the National Energy Research Scientific Computing Center, a DOE Office of Science User Facility supported by the Office of Science of the U.S. Department of Energy under Contract No. DE-AC02-05CH11231. This work was also supported by the South Carolina Smart State Center for Strategic Approaches to the Generation of Electricity (SAGE).

References

- Corma, A.; Iborra, S.; Velty, A., Chemical Routes for the Transformation of Biomass into Chemicals.
 Chem. Rev. 2007, 107, 2411-2502.
- 2. Serrano-Ruiz, J. C.; Luque, R.; Sepulveda-Escribano, A., Transformations of biomass-derived platform molecules: from high added-value chemicals to fuelsvia aqueous-phase processing. *Chem. Soc. Rev.* **2011**, *40*, 5266-5281.
- 3. Climent, M. J.; Corma, A.; Iborra, S., Conversion of biomass platform molecules into fuel additives and liquid hydrocarbon fuels. *Green Chem.* **2014**, *16*, 516.
- 4. Yi, J.; Liu, S.; Abu-Omar, M. M., Rhenium-Catalyzed Transfer Hydrogenation and Deoxygenation of Biomass-Derived Polyols to Small and Useful Organics. *ChemSusChem* **2012**, *5*, 1401-1404.
- Ota, N.; Tamura, M.; Nakagawa, Y.; Okumura, K.; Tomishige, K., Hydrodeoxygenation of vicinal
 OH groups over heterogeneous rhenium catalyst promoted by palladium and ceria support. *Angew. Chem. Int. Ed.* 2015, *54*, 1897-900.
- 6. Sousa, S. C. A.; Fernandes, A. C., Efficient deoxygenation methodologies catalyzed by oxomolybdenum and oxo-rhenium complexes. *Coord. Chem. Rev.* **2015**, *284*, 67-92.
- 7. Mamun, O.; Saleheen, M.; Bond, J. Q.; Heyden, A., Importance of Angelica Lactone Formation in the Hydrodeoxygenation of Levulinic Acid to γ-Valerolactone over a Ru(0001) Model Surface. *J. Phys. Chem. C* 2017, *121*, 18746-18761.
- 8. Lin, Z.; Chen, R.; Qu, Z.; Chen, J. G., Hydrodeoxygenation of biomass-derived oxygenates over

metal carbides: from model surfaces to powder catalysts. Green Chem. 2018, 20, 2679-2696.

- 9. Wang, C.; Mironenko, A. V.; Raizada, A.; Chen, T.; Mao, X.; Padmanabhan, A.; Vlachos, D. G.; Gorte, R. J.; Vohs, J. M., Mechanistic Study of the Direct Hydrodeoxygenation of m-Cresol over WOx-Decorated Pt/C Catalysts. *ACS Catal.* **2018**, *8*, 7749-7759.
- 10. Cook, G. K.; Andrews, M. A., Toward Nonoxidative Routes to Oxygenated Organics: Stereospecific Deoxydehydration of Diols and Polyols to Alkenes and Allylic Alcohols Catalyzed by the Metal Oxo Complex (C5Me5)ReO3. *J. Am. Chem. Soc.* **1996,** *118,* 9448-9449.
- 11. Ota, N.; Tamura, M.; Nakagawa, Y.; Okumura, K.; Tomishige, K., Performance, Structure, and Mechanism of ReOx–Pd/CeO2Catalyst for Simultaneous Removal of Vicinal OH Groups with H2. *ACS Catal.* **2016**, *6*, 3213-3226.
- 12. Sandbrink, L.; Klindtworth, E.; Islam, H.-U.; Beale, A. M.; Palkovits, R., ReOx/TiO2: A Recyclable Solid Catalyst for Deoxydehydration. *ACS Catal.* **2016**, *6*, 677-680.
- 13. Petersen, A. R.; Fristrup, P., New Motifs in Deoxydehydration: Beyond the Realms of Rhenium. *Chem. Eur. J.* **2017**, *23*, 10235-10243.
- 14. Xi, Y. J.; Yang, W. Q.; Ammal, S. C.; Lauterbach, J.; Pagan-Torres, Y.; Heyden, A., Mechanistic study of the ceria supported, re-catalyzed deoxydehydration of vicinal OH groups. *Catal. Sci. Technol.* **2018,** *8*, 5740-5752.
- 15. Donnelly, L. J.; Thomas, S. P.; Love, J. B., Recent Advances in the Deoxydehydration of Vicinal Diols and Polyols. *Chem. Asian J.* **2019**, *14*, 3782-3790.
- 16. Sandbrink, L.; Beckerle, K.; Meiners, I.; Liffmann, R.; Rahimi, K.; Okuda, J.; Palkovits, R., Supported Molybdenum Catalysts for the Deoxydehydration of 1,4-Anhydroerythritol into 2,5-Dihydrofuran. *ChemSusChem* **2017**, *10*, 1375-1379.

- 17. Gopaladasu, T. V.; Nicholas, K. M., Carbon Monoxide (CO)- and Hydrogen-Driven, Vanadium-Catalyzed Deoxydehydration of Glycols. *ACS Catal.* **2016**, *6*, 1901-1904.
- 18. Denning, A. L.; Dang, H.; Liu, Z.; Nicholas, K. M.; Jentoft, F. C., Deoxydehydration of Glycols Catalyzed by Carbon-Supported Perrhenate. *ChemCatChem* **2013**, *5*, 3567-3570.
- 19. Jang, J. H.; Sohn, H.; Camacho-Bunquin, J.; Yang, D.; Park, C. Y.; Delferro, M.; Abu-Omar, M. M., Deoxydehydration of Biomass-Derived Polyols with a Reusable Unsupported Rhenium Nanoparticles Catalyst. *ACS Sustainable Chem. Eng.* **2019**, *7*, 11438-11447.
- 20. Nakagawa, Y.; Tazawa, S.; Wang, T.; Tamura, M.; Hiyoshi, N.; Okumura, K.; Tomishige, K., Mechanistic Study of Hydrogen-Driven Deoxydehydration over Ceria-Supported Rhenium Catalyst Promoted by Au Nanoparticles. *ACS Catal.* **2018**, *8*, 584-595.
- 21. Qiao, B.; Wang, A.; Yang, X.; Allard, L. F.; Jiang, Z.; Cui, Y.; Liu, J.; Li, J.; Zhang, T., Single-atom catalysis of CO oxidation using Pt1/FeOx. *Nat. Chem.* **2011**, *3*, 634-641.
- Kyriakou, G.; Boucher, M. B.; Jewell, A. D.; Lewis, E. A.; Lawton, T. J.; Baber, A. E.; Tierney, H. L.; Flytzani-Stephanopoulos, M.; Sykes, E. C. H., Isolated Metal Atom Geometries as a Strategy for Selective Heterogeneous Hydrogenations. *Science* 2012, *335*, 1209-1212.
- 23. Jones, J.; Xiong, H.; DeLaRiva, A. T.; Peterson, E. J.; Pham, H.; Challa, S. R.; Qi, G.; Oh, S.; Wiebenga, M. H.; Pereira Hernández, X. I.; Wang, Y.; Datye, A. K., Thermally stable single-atom platinum-on-ceria catalysts via atom trapping. *Science* **2016**, *353*, 150-154.
- 24. Wang, A. Q.; Li, J.; Zhang, T., Heterogeneous single-atom catalysis. *Nat. Rev. Chem.* **2018**, *2*, 65-81.
- Li, H.; Wang, L.; Dai, Y.; Pu, Z.; Lao, Z.; Chen, Y.; Wang, M.; Zheng, X.; Zhu, J.; Zhang, W.; Si,
 R.; Ma, C.; Zeng, J., Synergetic interaction between neighbouring platinum monomers in CO2

hydrogenation. Nature Nanotech. 2018, 13, 411-417.

- 26. Tian, S.; Fu, Q.; Chen, W.; Feng, Q.; Chen, Z.; Zhang, J.; Cheong, W.-C.; Yu, R.; Gu, L.; Dong, J.; Luo, J.; Chen, C.; Peng, Q.; Draxl, C.; Wang, D.; Li, Y., Carbon nitride supported Fe2 cluster catalysts with superior performance for alkene epoxidation. *Nat. Commun.* **2018**, *9*, 2353.
- 27. Zhao, Y.; Yang, K. R.; Wang, Z.; Yan, X.; Cao, S.; Ye, Y.; Dong, Q.; Zhang, X.; Thorne, J. E.; Jin, L.; Materna, K. L.; Trimpalis, A.; Bai, H.; Fakra, S. C.; Zhong, X.; Wang, P.; Pan, X.; Guo, J.; Flytzani-Stephanopoulos, M.; Brudvig, G. W.; Batista, V. S.; Wang, D., Stable iridium dinuclear heterogeneous catalysts supported on metal-oxide substrate for solar water oxidation. *Proc. Natl. Acad. Sci. U.S.A.* 2018, *115*, 2902-2907.
- 28. Hunter, M. A.; Fischer, J. M. T. A.; Yuan, Q.; Hankel, M.; Searles, D. J., Evaluating the Catalytic Efficiency of Paired, Single-Atom Catalysts for the Oxygen Reduction Reaction. *ACS Catal.* **2019**, 7660-7667.
- 29. Jiao, J.; Lin, R.; Liu, S.; Cheong, W.-C.; Zhang, C.; Chen, Z.; Pan, Y.; Tang, J.; Wu, K.; Hung, S.-F.; Chen, H. M.; Zheng, L.; Lu, Q.; Yang, X.; Xu, B.; Xiao, H.; Li, J.; Wang, D.; Peng, Q.; Chen, C.; Li, Y., Copper atom-pair catalyst anchored on alloy nanowires for selective and efficient electrochemical reduction of CO2. *Nature Chem.* **2019**, *11*, 222-228.
- 30. Ye, W.; Chen, S.; Lin, Y.; Yang, L.; Chen, S.; Zheng, X.; Qi, Z.; Wang, C.; Long, R.; Chen, M.; Zhu, J.; Gao, P.; Song, L.; Jiang, J.; Xiong, Y., Precisely Tuning the Number of Fe Atoms in Clusters on N-Doped Carbon toward Acidic Oxygen Reduction Reaction. *Chem* **2019**, *5*, 2865-2878.
- 31. Park, S.; Park, J.; Abroshan, H.; Zhang, L.; Kim, J. K.; Zhang, J.; Guo, J.; Siahrostami, S.; Zheng, X., Enhancing Catalytic Activity of MoS2 Basal Plane S-Vacancy by Co Cluster Addition. *ACS Energy Letters* **2018**, *3*, 2685-2693.

- 32. Li, H.; Tsai, C.; Koh, A. L.; Cai, L.; Contryman, A. W.; Fragapane, A. H.; Zhao, J.; Han, H. S.; Manoharan, H. C.; Abild-Pedersen, F.; Nørskov, J. K.; Zheng, X., Activating and optimizing MoS2 basal planes for hydrogen evolution through the formation of strained sulphur vacancies. *Nature Mater.* **2015**, *15*, 48.
- 33. Wang, X.; Zhang, Y.; Si, H.; Zhang, Q.; Wu, J.; Gao, L.; Wei, X.; Sun, Y.; Liao, Q.; Zhang, Z.; Ammarah, K.; Gu, L.; Kang, Z.; Zhang, Y., Single-Atom Vacancy Defect to Trigger High-Efficiency Hydrogen Evolution of MoS2. *J. Am. Chem. Soc.* **2020**, *142*, 4298-4308.
- 34. Wang, Z.; Zhao, J.; Cai, Q.; Li, F., Computational screening for high-activity MoS2 monolayer-based catalysts for the oxygen reduction reaction via substitutional doping with transition metal. *J. Mater. Chem. A* **2017**, *5*, 9842-9851.
- 35. Liu, G.; Robertson, A. W.; Li, M. M.-J.; Kuo, W. C. H.; Darby, M. T.; Muhieddine, M. H.; Lin, Y.-C.; Suenaga, K.; Stamatakis, M.; Warner, J. H.; Tsang, S. C. E., MoS2 monolayer catalyst doped with isolated Co atoms for the hydrodeoxygenation reaction. *Nature Chem.* **2017**, *9*, 810.
- 36. Kresse, G.; Furthmuller, J., Efficient iterative schemes for ab initio total-energy calculations using a plane-wave basis set. *Phys. Rev. B* **1996**, *54*, 11169.
- 37. Kresse, G.; Furthmuller, J., Efficiency of ab-initio total energy calculations for metals and semiconductors using a plane-wave basis set. *Comput. Mater. Sci.* **1996,** *6*, 15-50.
- 38. Perdew, J. P.; Burke, K.; Ernzerhof, M., Generalized gradient approximation made simple. *Phys. Rev. Lett.* **1996,** *77*, 3865.
- 39. Blochl, P. E., Projector augmented-wave method. Phys. Rev. B 1994, 50, 17953-17979.
- 40. Kresse, G.; Joubert, D., From ultrasoft pseudopotentials to the projector augmented-wave method. *Phys. Rev. B* **1999**, *59*, 1758-1775.

- 41. Monkhorst, H. J.; Pack, J. D., Special Points for Brillouin-Zone Integrations. *Phys. Rev. B* **1976**, *13*, 5188.
- 42. Grimme, S.; Antony, J.; Ehrlich, S.; Krieg, H., A consistent and accurate ab initio parametrization of density functional dispersion correction (DFT-D) for the 94 elements H-Pu. *J. Chem. Phys.* **2010**, *132*, 154104.
- 43. Henkelman, G.; Uberuaga, B. P.; Jonsson, H., A climbing image nudged elastic band method for finding saddle points and minimum energy paths. *J. Chem. Phys.* **2000**, *113*, 9901-9904.
- 44. Henkelman, G.; Jónsson, H., A dimer method for finding saddle points on high dimensional potential surfaces using only first derivatives. *J. Chem. Phys.* **1999**, *111*, 7010-7022.
- 45. Heyden, A.; Bell, A. T.; Keil, F. J., Efficient methods for finding transition states in chemical reactions: comparison of improved dimer method and partitioned rational function optimization method. *J. Chem. Phys.* **2005**, *123*, 224101.
- 46. Jellinek, F.; Brauer, G.; MÜLler, H., Molybdenum and Niobium Sulphides. *Nature* **1960,** *185*, 376-377.
- 47. Saleheen, M.; Zare, M.; Faheem, M.; Heyden, A., Computational Investigation of Aqueous Phase Effects on the Dehydrogenation and Dehydroxylation of Polyols over Pt(111). *J. Phys. Chem. C* **2019**, *123*, 19052-19065.
- 48. Behtash, S.; Lu, J.; Faheem, M.; Heyden, A., Solvent effects on the hydrodeoxygenation of propanoic acid over Pd(111) model surfaces. *Green Chem.* **2014**, *16*, 605-616.
- 49. Liu, J.-C.; Tang, Y.; Wang, Y.-G.; Zhang, T.; Li, J., Theoretical understanding of the stability of single-atom catalysts. *Natl. Sci. Rev.* **2018**, *5*, 638-641.
- 50. Antoine Equation Parameters of 1,2-Ethanediol. https://webbook.nist.gov/chemistry/ (accessed

Jan. 23).

- 51. Campbell, C. T., The Degree of Rate Control: A Powerful Tool for Catalysis Research. *ACS Catal.* **2017,** *7*, 2770-2779.
- 52. Stanowski, S.; Nicholas, K. M.; Srivastava, R. S., [Cp*Ru(CO)2]2-Catalyzed Hydrodeoxygenation and Hydrocracking of Diols and Epoxides. *Organometallics* **2012**, *31*, 515-518.
- 53. Shan, C.; Zhu, L.; Qu, L.-B.; Bai, R.; Lan, Y., Mechanistic view of Ru-catalyzed C–H bond activation and functionalization: computational advances. *Chem. Soc. Rev.* **2018**, *47*, 7552-7576.
- 54. Pan, S.; Shibata, T., Recent Advances in Iridium-Catalyzed Alkylation of C–H and N–H Bonds. *ACS Catal.* **2013,** *3*, 704-712.
- 55. Wu, D.; Zhang, Y.; Su, H., Mechanistic Study on Oxorhenium-Catalyzed Deoxydehydration and Allylic Alcohol Isomerization. *Chem. Asian J.* **2016,** *11*, 1565-1571.

TOC figure

